ELSEVIER

Chemical Engineering Journal 137 (2008) 328–338

Chemical Engineering Journal

www.elsevier.com/locate/cej

Effect of heating rate on liquefaction of cellulose by hot compressed water

Eiji Kamio [a], Susumu Takahashi [a], Hidehiko Noda [b], Chouji Fukuhara [a], Takanari Okamura [a,*]

[a] *Department of Chemical Engineering on Biological Environment, Hachinohe Institute of Technology, 88-1 Ohiraki, Myo, Hachinohe 031-8501, Japan*
[b] *Department of Mechanical Engineering, Hachinohe Institute of Technology, 88-1 Ohiraki, Myo, Hachinohe 031-8501, Japan*

Received 20 August 2006; received in revised form 7 April 2007; accepted 2 May 2007

Abstract

The effect of heating rate on the liquefaction of a microcrystalline cellulose particle was investigated by using a batch type reactor with a temperature controller. Experiments were carried out over the temperature range of 443–553 K. The temperature profile of the heating was controlled to obtain a proportional relationship with time. Heating rates ranged from 0.0167 to 0.167 K/s. The resulting concentration profiles of cellulose, oligosaccharides, monosaccharides and pyrolysis products were analyzed using a theoretical model which considered temperature variation during the reaction. The calculated results exhibit a reasonable fit to the experimental data. The predicted cellulose concentration profiles over a wide range of heating rates indicate that liquefaction of cellulose is affected when the heating rate is below 1 K/s. It is concluded that consideration of the heating process is necessary in the modeling of liquefaction when using reactors which cannot achieve fast heating.

Keywords: Hot compressed water; Heating rate; Liquefaction; Cellulose; Reaction kinetics; Process design

1. Introduction

Supercritical, subcritical and hot compressed water have been widely investigated and developed as technologies for converting wood biomass with high moisture contents to fuels [1–7]. One advantage of these technologies is that they do not require a drying process for wood biomass. Because the water contained in wood biomass is used as a solvent as well as a reactant in these technologies, the drying process, which is required in the conventional gasification process and has a high energy cost, is not required for the conversion of wet biomass. The other advantage is that water results in a faster reaction under high temperature and high-pressure conditions. The reaction rate is easily and continuously controlled by controlling the temperature and pressure of the system. These technologies are also advantageous from an environmental point of view. Conventional manufacturing techniques for wood biomass treatment are not environmentally friendly as they use alkali and acid aqueous solutions for pulping and bleaching treatments, and special solvents for dissolution. On the other hand, in the technologies using supercritical, subcritical and hot compressed water, the complete decomposition of wood biomass and its related organics is achieved without any additives or catalysts by controlling the operating conditions such as temperature and residence time [8–11]. Only water is necessary for these technologies.

Wood biomass is typically composed of cellulose, hemicellulose and lignin. A variety of aqueous processes have been developed to separate these components from whole biomass [12–15]. It has been reported that hemicellulose and lignin undergo solvolysis with hot compressed water at temperatures above 463 K [12]. Cellulose is one of the most difficult components to dissolve in hot water. Cellulose is a homopolymer, in which 100–3000 glucose residues are linearly combined. The cellulose molecules are bound to each other by intermolecular and intramolecular hydrogen linkages through their hydroxyl groups. Therefore, cellulose molecules form crystal structures under normal conditions and crystalline cellulose is difficult to decompose. Even for such stable crystalline cellulose, however, both supercritical water and hot compressed water produce significant gasification and liquefaction. Minowa et al. investigated the liquefaction and gasification of cellulose by hot compressed water [10]. They investigated the effect of temperature on cellulose decomposition and reported that cellulose was completely decomposed at 553 K. Sasaki et al. investigated cellulose reforming with subcritical and supercritical water [16–20]. They achieved remarkably rapid decomposition of cellulose, in the order of several seconds or less, without using catalysis.

* Corresponding author. Tel.: +81 178 25 8089; fax: +81 178 25 8015.
E-mail address: okamura@hi-tech.ac.jp (T. Okamura).

1385-8947/$ – see front matter © 2007 Elsevier B.V. All rights reserved.
doi:10.1016/j.cej.2007.05.007

Nomenclature

C_b	concentration of water monomer in the bulk (mol/m^3)
C_e	concentration of chemicals after the reaction (mol/m^3)
C_i	concentration of chemicals (mol/m^3)
C_s	concentration of water monomer at the surface of cellulose particle (mol/m^3)
D	diffusion coefficient of water (m^2/s)
DP	degree of polymerization
E_{ai}	activation energy (kJ/mol)
h	time interval set for the calculation of the fourth-order Runge–Kutta method (s)
k_{0i}	frequency factor for reactions (9)–(11) (s^{-1})
k_{0s}	frequency factor for reaction (8) (m/s)
k_1	apparent rate constant of cellulose decomposition (mol$^{1/3}$/(m s))
k_2	rate constant of Eq. (2) (1/s)
k_3	rate constant of Eq. (3) (1/s)
k_4	rate constant of Eq. (4) (1/s)
k_c	mass transfer coefficient of water monomer through the aqueous film surrounding a cellulose particle (m/s)
k_s	first-order rate constant of hydrolysis reaction for cellulose decomposition (m/s)
m	recovered weight of cellulose particle (g)
m_0	loaded weight of cellulose particle (g)
r	radial position of cellulose surface (m)
r_A	apparent reaction rate of water monomer for unit cellulose particle (mol/s)
r_B	apparent reaction rate of cellulose molecule for unit cellulose particle (mol/s)
r_{Cel}	decomposition rate of cellulose particle (mol/(m^3 s))
$r_{Oligo,d2}$	decomposition rate of oligosaccharides to monosaccharides (mol/(m^3 s))
$r_{Oligo,d4}$	decomposition rate of oligosaccharides to pyrolysis products (mol/(m^3 s))
$r_{Pyro,f3}$	formation rate of pyrolysis products from monosaccharides (mol/(m^3 s))
$r_{Pyro,f4}$	formation rate of pyrolysis products from oligosaccharides (mol/(m^3 s))
r_i	overall reaction rate of chemicals (mol/(m^3 s))
$r_{i,d}$	total decomposition rate of chemicals (mol/(m^3 s))
$r_{i,f}$	total formation rate of chemicals (mol/(m^3 s))
r_0	radius of unreacted cellulose particle (m)
r_1	reaction rate of elementary process shown as Eq. (1) (mol/(m^3 s))
r_2	reaction rate of elementary process shown as Eq. (2) (mol/(m^3 s))
r_3	reaction rate of elementary process shown as Eq. (3) (mol/(m^3 s))
r_4	reaction rate of elementary process shown as Eq. (4) (mol/(m^3 s))
R	gas constant (J/(mol K))
t	time (s)
t_m	time when T reaches T_{max} (s)
T	temperature (K)
T_{init}	initial temperature (K)
T_{max}	maximum temperature set as an experimental condition (K)
v_T	heating rate (K/s)
V	volume of the reactor (m^3)
W_A	mass transfer rate of water monomer (mol/s)
W_B	hydrolysis reaction rate at the surface of a cellulose particle (mol/s)
x	decomposition ratio of unit cellulose particle

Greek letters

δ	thickness of aqueous film surrounding a cellulose particle (m)
ρ	molar density of the cellulose particle (mol/m^3)

Subscripts

Cel	cellulose
d	decomposition
DP	degree of polymerization
f	formation
Fru	fructose
Glu	glucose
Mono	monosaccharides
Oligo	oligosaccharides
Pyro	pyrolysis products
1–4	reaction described in Eqs. (1)–(4)

The practical use of technologies using supercritical, subcritical and hot compressed water for reforming wood biomass should be possible in the near future. However, there are still some difficulties that need to be overcome before these technologies can be adopted into practical use. One of the most important subjects in this respect is the development of adequate modeling for the processes. Although many researchers have been investigating gasification and liquefaction of wood biomass using these technologies, to our knowledge, only a few studies on the modeling of these processes have been carried out. Kabyemela et al. tried modeling the decomposition of wood biomass-related water soluble organics such as glucose, dihydroxyacetone and glyceraldehyde in subcritical and supercritical water [21,22]. In their research, they used an experimental setup with a compact flow-type reactor. The compact reactor simplifies the modeling of the process: a steady state is easily created, because rapid heating and quick quenching can be achieved. The model they proposed is very useful. However, practical use of a compact reactor for reforming wood biomass has one important shortcoming: solid wood biomass having a large particle diameter cannot be fed into the narrow channel. On the other hand, in a practical operation for the treatment of solid wood biomass, a batch type reactor is preferable from

an aspect of a treatment of solid wood biomass with an easy operation and a simple model. In this study, we examine liquefaction of a solid sample by using a batch reactor. Once the solid sample is liquefied, we can adopt a compact device for subsequent treatment. However, in the actual process of liquefaction of solid biomass by batch reactor, it is difficult to achieve quick heating and rapid quenching. Although it is important to know the reaction profile which accompanies the heating and quenching processes in a batch reactor, there is no study modeling such a system. The aim of this study is to estimate the reaction profile of solid cellulose, as a model sample of wood biomass, in a batch reactor under various heating rates. The batch reactor equips a temperature controller but cannot achieve quick heating and rapid quenching. The effect of the heating rate on the liquefaction of solid cellulose particles in hot compressed water is measured experimentally and predicted theoretically. The fundamental findings from this investigation should help in the design of not only batch reactors but also flow-type reactors.

2. Experimental

2.1. Reagents

The cellulose used in this work was de-ashed microcrystalline cellulose (Avicel No. 2331; average particle diameter 20–100 μm) purchased from Merck. The reagents used for the high performance liquid chromatography (HPLC) analysis were as follows: cellobiose (>99%), cellotriose (>98%), cellotetraose (>95%), cellopentaose (>95%), erythrose (50%), pyrvaldehyde (40%), glyceraldehyde (>95%) and 5-hydroxymethyl-2-furaldehyde (5-HMF) (>99%) (from Sigma–Aldrich Japan K.K. Co. Ltd., Tokyo); and glucose (>99%) and fructose (>99%) (from Wako Pure Chemicals Industries Ltd. (Osaka)).

2.2. Cellulose liquefaction experiments and product analysis

A schematic of the batch reactor system is presented in Fig. 1. A standard 9.7×10^{-5} m^3 reactor fabricated from Hastelloy C-22 and equipped with a stirring shaft and four cartridge heaters was used. The reactor had two type K thermocouples, to measure the temperature of the inner aqueous phase and that of the reactor wall in which the cartridge heaters were stuck. The thermocouples and the cartridge heaters were connected to the system controller. The temperature was controlled by PDI according to the temperature profile which was set by a computer program. The monitored temperatures were recorded in a notebook PC. The reactor was also equipped with a pressure indicator and a N_2 line to purge the air. The system was configured with pressure and temperature alarms which turned off the furnace if the pressure or temperature exceeded the preset limit. The batch system was also equipped with a gas sampling system. After the reaction, the gas produced was collected with a diaphragm pump and analyzed by gas chromatography (Shimadzu, GC-2014). Carbon dioxide and oxygen gas were detected when the maximum temperature was over 533 K, but their quantities were extremely low (below 7×10^{-4} mol even when the maximum temperature was set at 553 K). Therefore, in this study, the gas produced was neglected in the data treatment.

The liquefaction experiment was carried out as follows. A 0.7 g sample of cellulose and 69.3 g of ultra pure water were introduced into the reactor cell. The reactor cell was attached to the system and sealed. The reactor was purged, pressurized with N_2 gas to 1 MPa, and checked for leaks. This high loading of N_2 gas prevented evaporation of water. The stirrer was then started, and the reactor and its contents were heated according to the pre-set temperature program. In this study, the heating rate of the aqueous medium, v_T, was set at 0.0167, 0.0333, 0.050, 0.0667, 0.10 or 0.1667 K/s. The maximum temperature, T_{max}, was set at 443, 473, 493, 503, 513, 523, 533 or 553 K. As soon

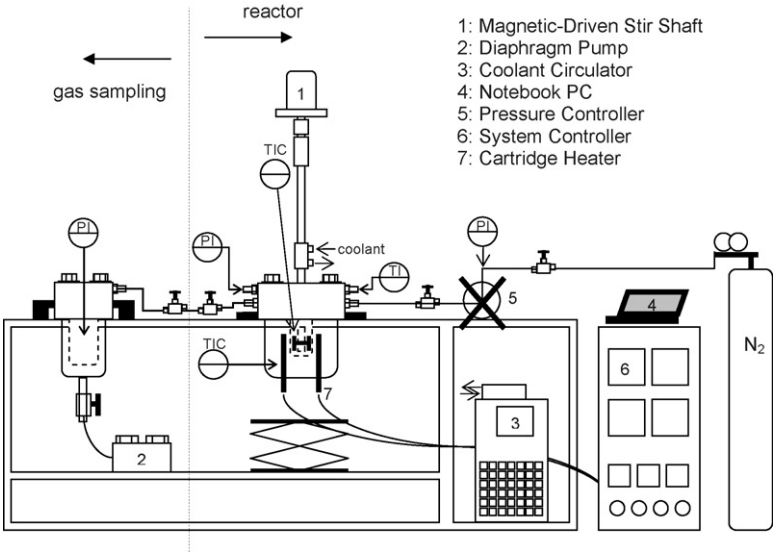

Fig. 1. Schematic of batch reactor system.

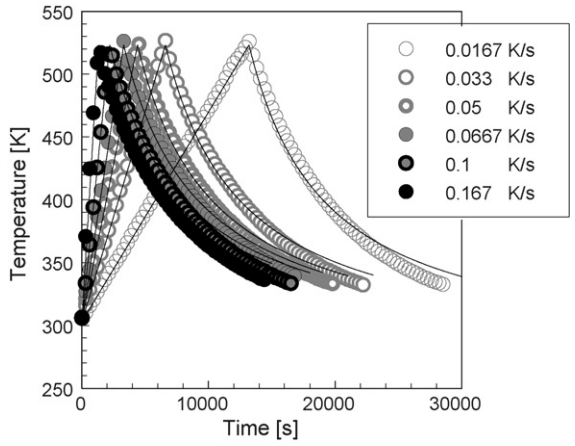

Fig. 2. Comparison of experimental and calculated temperature profile of the aqueous phase inside the cell. Plots: experimental data, solid lines: calculated data. The heating rate is 0.0167–0.167 K/s. The quenching is done by natural cooling.

as the medium temperature reached the maximum temperature, the heating was stopped. The reactor was subsequently cooled by air-cooling at room temperature. Fig. 2 shows the temperature profiles of the aqueous media for each v_T at $T_{max} = 523$ K. After the reactor contents were fully cooled, the reactor cell was separated from the system. The entire contents of the reactor cell were collected. The collection ratios were over 99% for all experiments. The collected sample was then filtered through a PTFE membrane filter with a pore size of 0.5×10^{-6} m. The solid residue was dried at room temperature in a vacuum desiccator, and weighed. The decomposition ratio of the cellulose particle, x, was calculated from the mass balance of the solid sample before and after reaction:

$$x = \frac{m_0 - m}{m_0} \quad (1)$$

where m_0 is the total amount of cellulose introduced and m is the amount of cellulose recovered after the experiment. The composition of the liquid filtrate was analyzed by HPLC (Shimadzu Co. Ltd.). The HPLC equipment consisted of an isocratic pump (LC-10ADvp), an autosampler (SIL-10ADvp), and a system controller (SCL-10Avp). The column used for the analysis was a Shim-pack SPR-Ca. The HPLC was operated at an oven temperature of 358 K, with the flow of the water solvent being 1.0×10^{-8} m^3/s. The detector was a refractive index detector (RID-10A). Peak identification was established by using standard solutions of the pure compounds. Peak calibration was performed by using standard solutions of varying concentrations to develop a linear relationship between the peak areas and the corresponding concentrations.

We carried out all experiments twice and confirmed that the chromatogram and the obtained concentrations of each chemical are almost equal.

3. Results and discussion

Fig. 3 shows the relationship between x and T_{max} for various heating rates. Fig. 3 clearly indicates that the smaller

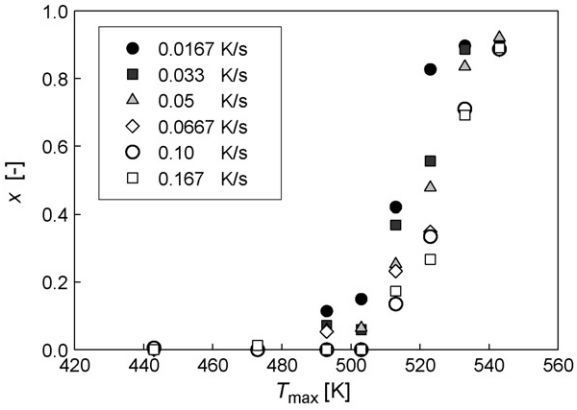

Fig. 3. Relationship between the decomposition ratio of cellulose and T_{max} for various v_T.

the heating rate, the more cellulose is decomposed. That is to say, under the experimental conditions we investigated, the heating rate strongly affects the cellulose decomposition rate. The HPLC chromatograms of the products at v_T = 0.0167, 0.033, 0.067, 0.10 and 0.167 K/s with $T_{max} = 523$ K are shown in Fig. 4(a). That of $v_T = 0.05$ K/s at $T_{max} = 523$ K is also shown in Fig. 4(b) with the retention times of the pure chemicals, which are indicated by vertical broken lines. As shown in Fig. 4(a), the concentration of glucose increased when the heat-

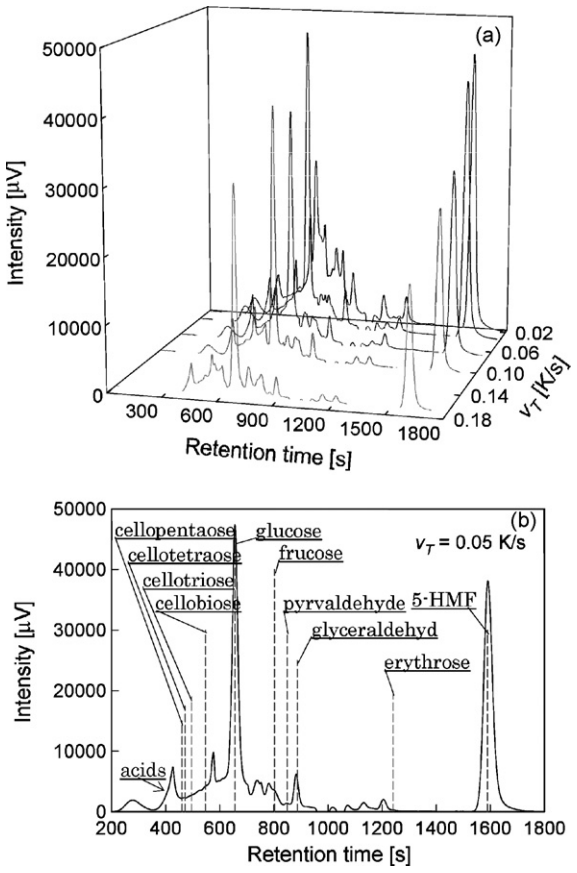

Fig. 4. HPLC chromatograms of recovered liquid samples. (a) Results for several v_T at $T_{max} = 523$ K. (b) Result at $v_T = 0.05$ K/s and $T_{max} = 523$ K and retention times of pure chemicals.

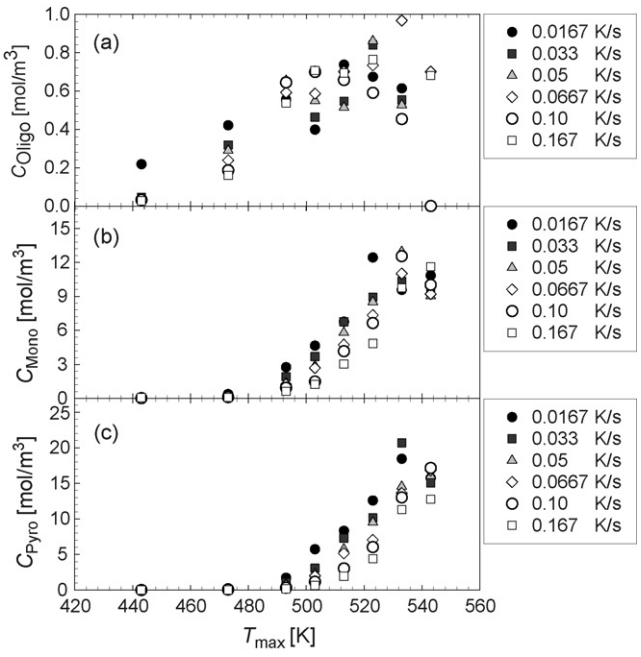

Fig. 5. Relationship between the concentration of products and T_{max} for various v_T: (a) oligosaccharides, (b) monosaccharides and (c) pyrolysis products.

ing rate was decreased from 0.167 to 0.033 K/s, but decreased when the heating rate was decreased from 0.033 to 0.0167 K/s. On the other hand, the concentrations of glyceraldehydes and 5-HMF, which are written as pyrolysis products in this study, monotonously increased with decreasing heating rates under the experimental conditions investigated. Variations in the concentrations of oligosaccharides, monosaccharides and pyrolysis products are summarized in Fig. 5(a)–(c), respectively. In these figures, C_{Oligo}, C_{Mono} and C_{Pyro} on the vertical axis are the concentrations of oligosaccharides, monosaccharides and pyrolysis products, respectively. They are defined by the following equations:

$$C_{Oligo} = \frac{\sum_{DP=2}^{5}(DP \cdot C_{Oligo,DP})}{3} \quad (2)$$

where DP means the degree of polymerization and $C_{Oligo,DP}$ gives the concentrations of cellobiose (DP = 2), cellotriose (DP = 3), cellotetraose (DP = 4) and cellopentanose (DP = 5). When calculating the oligosaccharide concentrations, we assumed that oligosaccharides consist of an average of three glucose units:

$$C_{Mono} = C_{Glu} + C_{Fru} \quad (3)$$

where C_{Glu} and C_{Fru} are the concentrations of glucose and fructose, respectively:

$$C_{Pyro} = C_{pyrvaldehyde} + C_{glyceraldehyde} + C_{erythrose} + C_{5\text{-HMF}} \quad (4)$$

In this study, we defined pyrolysis products as a generic term of products generated from the reactions except for hydrolysis reaction: pyrvaldehyde, glyceraldehydes, erythrose and 5-HMF. Therefore, C_{Pyro} can be defined as being the sum of those concentrations, as shown in Eq. (4). Although the dependence of the formation and decomposition of oligosaccharides on the heating rate as shown in Fig. 5(a) is not clear because of the experimental error in the HPLC analysis, the dependence of the reaction of monosaccharides and pyrolysis products on the heating rate, shown in Fig. 5(b) and (c), is evident. Under low T_{max} conditions, when T_{max} is below 533 K, the smaller the heating rates are, the more formation of monosaccharides and pyrolysis takes place. Around a T_{max} of 533 K, C_{Mono} resulting from a heating rate under 0.10 K/s shows a maximal value, but that using a heating rate of 0.167 K/s shows no peak. C_{Pyro} also shows a maximal value around a T_{max} of 533 K when the heating rate is below 0.033 K/s, but increases monotonically when the heating rate is above 0.05 K/s. These findings clearly indicate that the reaction rates of oligosaccharides, monosaccharides and pyrolysis products as well as the decomposition rate of cellulose are affected by the heating rate. In addition, by comparing Fig. 5(a)–(c), a simple and rough reaction pathway for cellulose decomposition using hot compressed water can be estimated. The cellulose particle decomposes according to the following stepwise processes—1, solid cellulose particle is hydrolyzed to oligosaccharides; 2, formed oligosaccharides decompose to both monosaccharides and pyrolysis products; 3, monosaccharides decompose to pyrolysis products; and 4, pyrolysis products are polymerized and form tar or char products. This suggested reaction pathway for cellulose decomposition with hot compressed water is the same as that in the model reported by Minowa et al. [10]. Under the experimental conditions investigated in this study, tar and char products were formed above a T_{max} of 533 K, but the quantities were quite small. As we cannot analyze the concentrations of tar and char products formed because of their small quantities and their complex chemical structures, we disregarded step 4 in the modeling of cellulose decomposition. In the following sections, we try to derive a mathematical model for the decomposition of cellulose with hot compressed water, based on the stepwise processes of steps 1–3. It should be noted that we propose a mathematical model which takes the dependence of the rate constants on the temperature validation during the heating and quenching processes into account: we represent the rate constant for each reaction as a function of temperature by using Arrhenius' law:

$$k_i = k_{0i} \exp\left(-\frac{E_{ai}}{RT}\right) \quad (5)$$

where k_i is the rate constant of the formation and decomposition reaction, and k_{0i} and E_{ai} are the general expressions for the frequency factor and the activation energy of the reaction. R is the gas constant, and T is the temperature, which is expressed as a function of time. To calculate the temperature profile, the following equations were used:

$$\text{heating process :} \quad T = v_T t + T_{init} \quad (6)$$

quenching process :

$$T = \frac{6000(T_{max} - 273.15)}{t - ((T_{max} - T_{init})/v_T) + 6000} + 273.15 \quad (7)$$

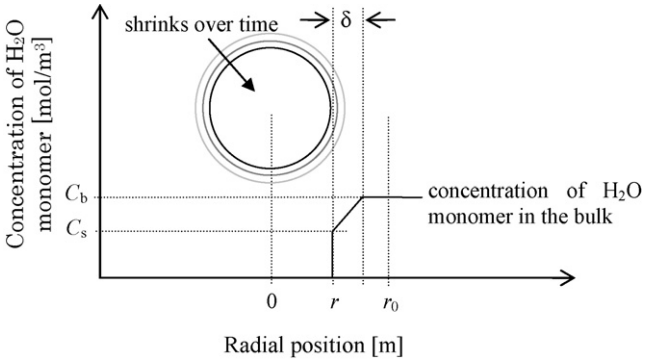

Fig. 6. Representation of the reacting cellulose particle proposed in this study.

where t is the time and T_{init} is the initial temperature, which is set at 303 K as an experimental condition. For Eq. (7), there is no actual physical inference, since this equation is used to describe the quenching profile by natural cooling. The solid lines in Fig. 2 are the temperature profiles calculated with Eqs. (6) and (7) for a T_{max} of 523 K. In the calculation, Eq. (6) is immediately changed to Eq. (7) when the temperature reaches T_{max}. As shown in Fig. 2, the calculated temperature profile describes the experimental data well.

In the derivation of the theoretical model, we assumed the following stoichiometric relationships:

$$\text{Cellulose(s)} + 75.7\text{H}_2\text{O(l)} \rightarrow 76.7\text{oligomer(l)}; \quad r_1 \tag{8}$$

$$\text{Oligomer(l)} + 2\text{H}_2\text{O(l)} \rightarrow 3\text{monomer(l)}; \quad r_2 \tag{9}$$

$$\text{Monomer(l)} + \text{H}_2\text{O(l)} \rightarrow \text{pyrolysis(l)}; \quad r_3 \tag{10}$$

$$\text{Oligomer(l)} + 2\text{H}_2\text{O(l)} \rightarrow 3\text{pyrolysis(l)}; \quad r_4 \tag{11}$$

In these equations, (s) and (l) mean the state of the materials: (s) is solid state and (l) is liquid state. Cellulose means a crystalline cellulose particle, which consists of an average of 230 molecules of glucose, because the crystalline cellulose used in this study has a viscosity averaged degree of polymerization of 230. It exists in an aqueous phase as a solid state. Oligomer, monomer and pyrolysis products mean the general term for oligosaccharides which consist of an average of three units of glucose, monosaccharides which consist of glucose and fructose, and pyrolysis products, respectively. r_1–r_4 are the reaction rates of each of the elementary processes. A first-order rate equation can be used for the chemical reactions of each process [19,21,22].

First we derived a mathematical expression for the cellulose decomposition. As reported by Sasaki et al. [17], a crystalline cellulose particle gradually shrinks at temperatures below 523 K. That is to say, the decomposition reaction of cellulose to oligosaccharides occurs at the particle surface of microcrystalline cellulose. It is a heterogeneous reaction. Therefore, the surface reaction model is used to describe the first process. A representation of the reacting cellulose particle as proposed in this study is shown in Fig. 6. In the mathematical derivation of the kinetic model, it is assumed that a cellulose particle is a spherical shape with an initial particle diameter of r_0. The chemical reaction of cellulose decomposition to oligosaccharides occurs at the surface of the cellulose particle [17,18]. The decomposition reaction of cellulose is hydrolysis by a water monomer. Water monomers are formed in both the aqueous bulk and the aqueous film near the cellulose particle, but are consumed in hydrolysis reactions at the surface of the cellulose particle. Therefore, a concentration gradient of water monomers is formed near the surface of the cellulose particle. A crystalline cellulose particle has no pores, so a water monomer cannot diffuse into the particle and the concentration of water monomers becomes 0 mol/m^3 at the cellulose particle surface. The following two steps occur in succession during decomposition of a cellulose particle: (A) diffusion of a water monomer through the aqueous film surrounding a cellulose particle to the surface of the particle, (B) hydrolysis reaction of a water monomer with a cellulose molecule at the surface of a cellulose particle. For the first mass-transfer step of the water monomer, we assumed a linear driving force approximation for the transportation of a water monomer from the bulk of the water to the surface of a cellulose particle. The mass transfer rate of the water monomer through the aqueous film is as follows:

$$W_A = 4\pi r^2 \cdot k_c(C_b - C_s) \tag{12}$$

where W_A is the mass transfer rate of the water monomer, C_b and C_s are the concentrations of water monomers in the bulk and at the surface of a cellulose particle, respectively, k_c the mass transfer coefficient of a water monomer through the aqueous film surrounding a cellulose particle, and r is the radial position of the cellulose surface after the reaction has started, which decreases as the hydrolysis reaction progresses. For the second hydrolysis reaction step, we assumed that the hydrolysis reaction rate could be expressed as a first-order reaction for water monomers. The hydrolysis reaction rate is expressed as follows:

$$W_B = 4\pi r^2 k_s \cdot C_s \tag{13}$$

where W_B is the hydrolysis reaction rate at the surface of a cellulose particle and k_s is the first-order rate constant, which varies during the reaction according to Eqs. (5)–(7). By assuming a quasi-steady state for the overall process of this cellulose decomposition, it is considered that Eqs. (12) and (13) are equal. In addition, they are considered to be equal to the apparent reaction rate of water monomer for one cellulose particle. Therefore, the following expression can be used:

$$-r_A = 4\pi r^2 \cdot k_c(C_b - C_s) = 4\pi r^2 k_s \cdot C_s \tag{14}$$

where r_A is the apparent reaction rate of water monomer for one cellulose particle. Eq. (14) can then be rewritten as the following equation:

$$-r_A = \frac{4\pi r^2 C_b}{1/k_c + 1/k_s} \tag{15}$$

Meanwhile, the decomposition rate is assessed by considering the mass balance of a cellulose particle. At a certain period during the reaction, the radial position of the cellulose surface becomes r, and the molar amount of cellulose particle remaining is $4\pi r^3 \cdot \rho/3$, where ρ is the molar density of the cellulose particle. At that time, the mass balance of the unit cellulose particle

is written as follows:

$$\frac{\mathrm{d}}{\mathrm{d}t}\left(\frac{4}{3}\pi r^3 \cdot \rho\right) = -r_\mathrm{B} \tag{16}$$

where r_B is the apparent reaction rate of the cellulose molecule for a unit cellulose particle. From the stoichiometric relationship of Eq. (8), $r_\mathrm{A} = 75.7 r_\mathrm{B}$. Therefore, from Eqs. (15) and (16), the following differential equation can be obtained:

$$-4\pi r^2 \cdot \rho \frac{\mathrm{d}r}{\mathrm{d}t} = \frac{4\pi r^2 C_\mathrm{b}}{75.7(1/k_\mathrm{c} + 1/k_\mathrm{s})} \tag{17}$$

This equation is the differential equation which expresses the variation of the radial position of the surface of a cellulose particle over time. We can transform Eq. (17) to a differential equation which expresses the variation in the decomposition ratio of the cellulose particle over time. When the radial position of the surface becomes r, the decomposition ratio of a cellulose particle is written as follows:

$$1 - x = \frac{4/3\pi r^3 \cdot \rho}{4/3\pi r_0^3 \cdot \rho} = \left(\frac{r}{r_0}\right)^3 \tag{18}$$

where x is the decomposition ratio of a unit cellulose particle. By differentiating Eq. (18) with respect to t, we obtain the following relationship:

$$-\frac{\mathrm{d}x}{\mathrm{d}t} = \frac{3}{r_0^3} r^2 \frac{\mathrm{d}r}{\mathrm{d}t} \tag{19}$$

By substituting Eqs. (18) and (19) into Eq. (17), we get the following differential equation which expresses the variation in the decomposition ratio of a cellulose particle over time:

$$\frac{4\pi r_0^3}{3}\rho \frac{\mathrm{d}x}{\mathrm{d}t} = \frac{4\pi r_0^2 (1-x)^{2/3} C_\mathrm{b}}{75.7(1/k_\mathrm{c} + 1/k_\mathrm{s})} \tag{20}$$

The decomposition ratio of a cellulose particle can be expressed by the concentration of cellulose molecules according to the following relationship:

$$x = \frac{C_{\mathrm{Cel},0} - C_\mathrm{Cel}}{C_{\mathrm{Cel},0}} \tag{21}$$

where $C_{\mathrm{Cel},0}$ and C_Cel are the concentrations of cellulose molecules at $t = 0$ and t, respectively. By substituting Eq. (21) into Eq. (20) and after simplification, we derive the decomposition rate equation of a cellulose particle as follows:

$$r_\mathrm{Cel} = -r_1 = \frac{\mathrm{d}C_\mathrm{Cel}}{\mathrm{d}t} = -k_1 C_\mathrm{Cel}^{2/3} \tag{22}$$

where r_Cel is the decomposition rate of a cellulose particle and k_1 is the apparent rate constant of cellulose decomposition described as follows:

$$k_1 = \frac{3C_{\mathrm{Cel},0}^{1/3} \cdot C_\mathrm{b}}{75.7\rho \cdot r_0 (1/k_\mathrm{c} + 1/k_\mathrm{s})} \tag{23}$$

In the calculation, it should be noted that the calculated concentration of cellulose is set at 0 mol/m^3 after it has obtained a negative value over time.

The mathematical expressions for oligomer, monomer, and pyrolysis products can now be derived. The reaction rates for Eqs. (9)–(11) can be expressed as first-order equations for the concentrations of oligomer and monomer. Therefore, the variations in the concentrations of oligomer, monomer and pyrolysis products with reaction time can be expressed by the following equations:

$$r_\mathrm{Oligo} = \frac{\mathrm{d}C_\mathrm{Oligo}}{\mathrm{d}t} = 76.7 r_1 - (r_2 + r_4) = 76.7 k_1 C_\mathrm{Cel}^{2/3} - (k_2 + k_4) C_\mathrm{Oligo} \tag{24}$$

$$r_\mathrm{Mono} = \frac{\mathrm{d}C_\mathrm{Mono}}{\mathrm{d}t} = 3r_2 - r_3 = 3k_2 C_\mathrm{Oligo} - k_3 C_\mathrm{Mono} \tag{25}$$

$$r_\mathrm{Pyro} = \frac{\mathrm{d}C_\mathrm{Pyro}}{\mathrm{d}t} = r_3 + 3r_4 = k_3 C_\mathrm{Mono} + 3k_4 C_\mathrm{Oligo} \tag{26}$$

where r_Oligo, r_Mono, and r_Pyro are the overall reaction rates of oligomer, monomer and pyrolysis products, respectively. k_2–k_4 are the rate constants for Eqs. (9)–(11), respectively. The rate constants k_2–k_4 also vary during the reaction according to Eqs. (5)–(7).

Variations in the concentrations of each product over time can be calculated by solving the obtained equations. However, it is impossible to solve the obtained equations analytically. Therefore, in this study, we solved the obtained equations numerically. In the numerical calculation, we adopted the fourth-order Runge–Kutta method. The parameters set in the calculation are shown in Table 1.

In Table 1, E_{ai} and k_{0i} are the fitting parameters which were determined so as to obtain a reasonable fit between the experimental data and the calculated results. In Table 2, activation energies reported in or determined from previously reported papers are shown. The activation energies used in this study, which are listed in Table 1, show a reasonable agreement with

Table 1
Parameters used in calculating the concentration of each chemical

Parameters	Set value	Unit
E_{as}	141	kJ/mol
E_{a2}	101	kJ/mol
E_{a3}	129	kJ/mol
E_{a4}	141	kJ/mol
k_{0s}	7.3	($\times 10^6$ m/s)
k_{02}	6.0	($\times 10^7$ s^{-1})
k_{03}	1.0	($\times 10^7$ s^{10})
k_{04}	3.0	($\times 10^7$ s^{11})
k_c	0.001	m/s
T_init	303.15	K
T_max	423.15–573.15 (changed in steps of 1 K)	K
C_Cel0	0.241	mol/m^3
r_0	8.0	($\times 10^{-5}$ m)
ρ	555	mol/m^3
m_0	0.7	g
V	7	($\times 10^{-5}$ m^3)
C_b	7.0	($\times 10^3$ mol/m^3)
R	8.314	J/(K mol)
h	1	s

Table 2
Activation energies as obtained from a literature study

Reaction	'Pressure (MPa)	E_a (kJ/mol)	Literature
Cellulose decomposition	30	136*	Sasaki [20]
Cellobiose hydrolysis	25	91**	Sasaki et al. [19]
Glucose decomposition	25–30	96	Kabyemela et al. [21]
	25	88	Amin et al. [23]
	25	121	Bobleter and Pape [24]
	25–30	133.6***	
Cellobiose pyrolysis	25	122.6	Sasaki et al. [19]

* Calculated from given data in Sasaki [20].
** Calculated from given data in Sasaki et al. [19].
*** Determined from the Arrhenius plot in which all data presented by Kabymela et al. [21], Amin et al. [23], and Bobleter and Pape [24] are plotted.

those from the literature, except for E_{a3}. The activation energy for glucose decomposition presented by Kabyemela et al. [21] is smaller than the E_{a3} used in the current study. However, when all values determined by Kabyemela et al. [21], Amin et al. [23] and Bobleter and Pape [24], which are shown in the figure presented by Kabyemela et al. [21], are used to determine the activation energy, we get 133.6 kJ/mol as the activation energy for glucose decomposition. This value is considerably closer to the E_{a3} used in this work. We also evaluated the validity of the frequency factor as well as the activation energy. The k_{0s} calculated from the given data in Sasaki [20] is 7.28×10^6 m/s. The k_{02} calculated from the given data in Sasaki et al. [19] is 2.83×10^7 s^{-1}. The k_{03} provided in Matsumura et al. [25] is 1.33×10^{10} s^{-1}. The k_{04} provided in Sasaki et al. [19] is 1.26×10^{11} s^{-1}. These values are almost the same as our setting values ($k_{0s} = 7.3 \times 10^6$, $k_{02} = 6.0 \times 10^7$, $k_{03} = 1.0 \times 10^{10}$ and $k_{04} = 3.0 \times 10^{11}$).

For the calculation, we set the concentration of water monomer at 7000 mol/m^3. Walrafen et al. measured the Raman OH stretching peak frequencies from water vapor below 647 K [26]. They concluded that the molar ratio of water monomer and dimmer at the critical point were ~0.3 and ~0.7, respectively. If the monomer ratio is 0.3, and there are only monomers and dimmers in the system, C_b is estimated about 9800 mol/m^3. Under the conditions investigated in this study, the temperature is below the critical point. Therefore, it is suggested that C_b is lower than 9800 mol/m^3. In another paper, Ohtomo et al. proposed a tetrahedrally coordinated pentamer–monomer model to estimate the liquid structure of water [27]. They concluded that the molar ratio of the water monomer and pentamer at 368 K were 0.45 and 0.55, respectively. If the monomer ratio is 0.45, and there are only monomers and pentamers in the system, C_b is estimated about 7000 mol/m^3. Under the conditions investigated in this study, the temperature is higher than 368 K. Therefore, it is suggested that C_b is higher than 7000 mol/m^3. From these estimations, it can be assumed that 7000 mol/m^3 is adequate for the monomer concentration of water. In the precalculation, we calculated the concentration profiles of cellulose, oligomer, monomer and pyrolysis for the range of C_b between 5000 and 10,000 mol/m^3 to compare the effects of C_b. As the result, we confirmed that the concentration profile varies just a little.

The other parameter k_c, which is the mass transfer coefficient of water monomer, was set at 0.001 m/s. The reason is as follows. The diffusion coefficient of water, D, is determined to about 1×10^{-8} m^2/s at 423 K and about 2.5×10^{-8} m^2/s at 523 K by Yoshida et al. with a high-resolution NMR probe method and MD simulation [28]. The k_c is the mass transfer coefficient which can be expressed as D/δ, where δ is thickness of the aqueous laminar film. In general, δ is estimated as 100 μm or less. In our experiment, we used microcrystalline cellulose particle having its diameter of about 80 μm. Therefore, it is considered that the δ is thinner than 80 μm. We assumed δ as 10 μm, therefore k_c is set at 0.001 m/s.

We compared the experimental results with the calculated ones for the proposed model. The theoretical calculation was carried out according to the following processes. At first, the cellulose concentration at $t = t_1$ and $T = T_1$, $C_{Cel,1}$, was calculated with $C_{Cel,0}$ and Eq. (22) in which Eqs. (5), (6) and (23) were substituted. With the obtained $C_{Cel,1}$, the oligomer concentration at $t = t_1$ and $T = T_1$, $C_{Oligo,1}$, was calculated with Eq. (24) in which Eqs. (5) and (6) were substituted. Similarly, $C_{Mono,1}$ and $C_{Pyro,1}$ were calculated in turn with Eqs. (25) and (26) in which Eqs. (5) and (6) were substituted, respectively. Subsequently, with the obtained $C_{Cel,1}$, the cellulose concentration at $t = t_2$ and $T = T_2$, $C_{Cel,2}$, was calculated in the same way for the calculation of $C_{Cel,1}$. In the calculation, we set the time interval, $h = t_{n+1} - t_n$, at 1 s. The $C_{Oligo,2}$, $C_{Mono,2}$ and $C_{Pyro,2}$ were also calculated in the same way for the calculation of $C_{Oligo,1}$, $C_{Mono,1}$ and $C_{Pyro,1}$, respectively. Similarly, the $C_{Cel,i}$, $C_{Oligo,i}$, $C_{Mono,i}$ and $C_{Pyro,i}$ were calculated one by one until t_m. The t_m was the time when T_i becomes $T_{max,1}$. After $t = t_{m+1}$, $C_{Cel,m+1}$ was calculated with $C_{Cel,m}$ and Eq. (22) in which Eqs. (5), (7) and (23) were substituted. The $C_{Oligo,m+1}$, $C_{Mono,m+1}$ and $C_{Pyro,m+1}$ were also calculated in turn with Eqs. (24)–(26) in which Eqs. (5) and (7) were substituted, respectively. The same calculation was continued until t became t_e which is the time when T_i value returned to T_{init}. The final concentrations of chemicals at $t = t_e$, $C_{Cel,e}$, $C_{Oligo,e}$, $C_{Mono,e}$ and $C_{Pyro,e}$, were obtained for $T_{max,1}$. A series of calculations were carried out for various $T_{max,i}$ from 430 to 550 K.

An example of a calculated result by Eqs. (22), (24)–(26) is shown in Fig. 7. In Fig. 7, we set $T_{max} = 523$ K and $v_T = 0.05$ K/s. Since we could not obtain the reactant concentrations

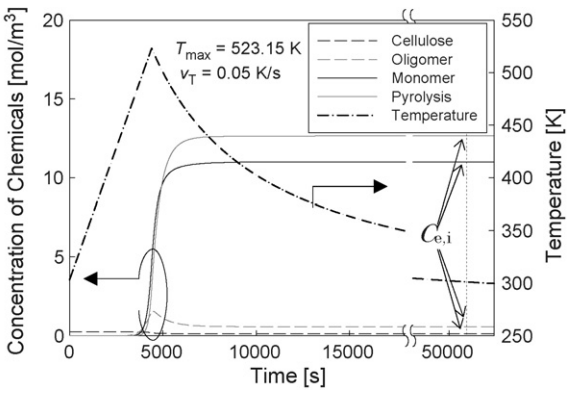

Fig. 7. An example of a calculated result. $T_{max} = 523$ K, $v_T = 0.05$ K/s.

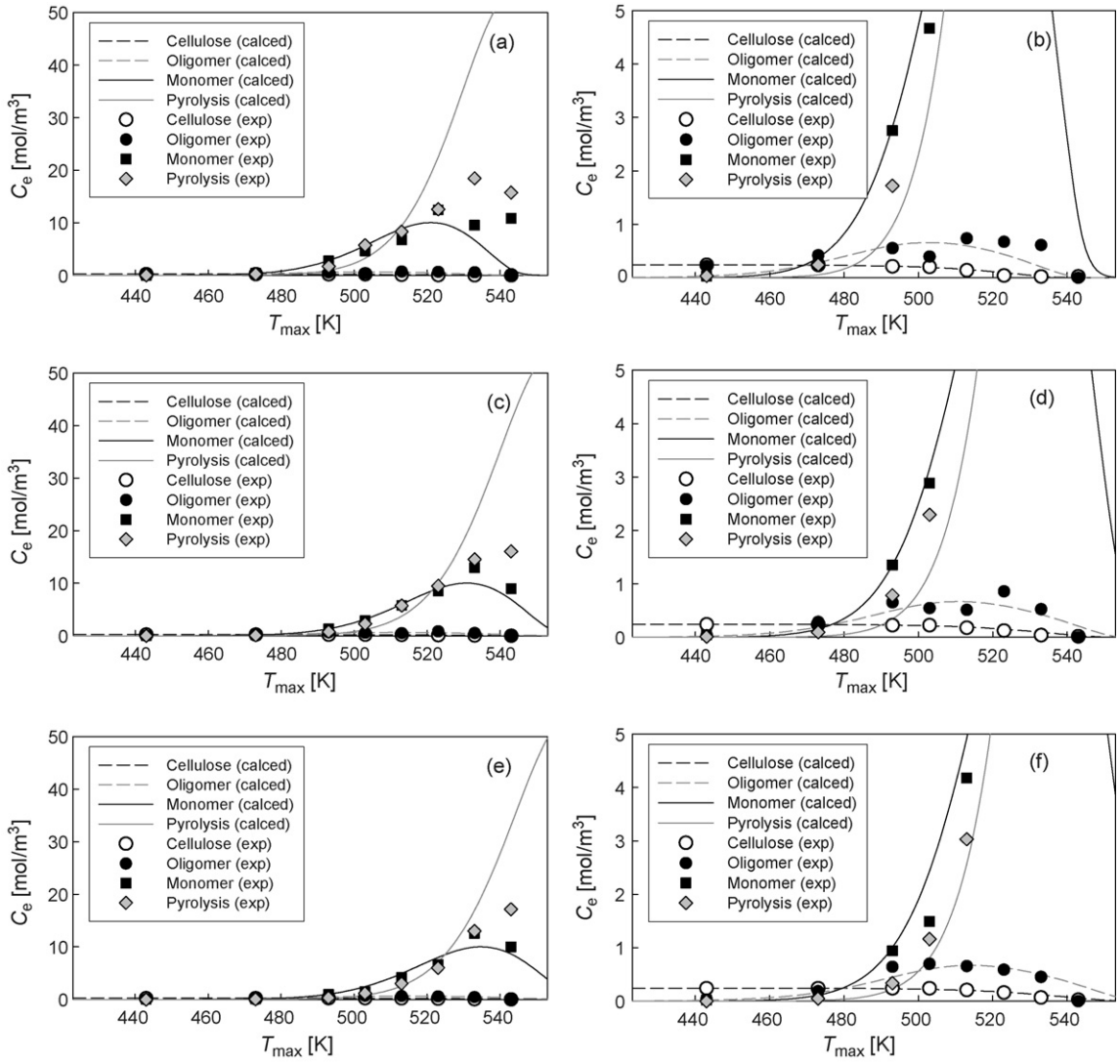

Fig. 8. Effect of T_{max} on C_e: (a) $v_T = 0.0167$ K/s, (b) Magnified part of the vertical axis in (a), (c) $v_T = 0.05$ K/s, (d) magnified part of the vertical axis in (c), (e) $v_T = 0.10$ K/s and (f) magnified part of the vertical axis in (e).

from our batch system in the middle of the operation, we had to investigate the effect of T_{max} and v_T on the concentration of chemicals after the reaction had stopped. Therefore, we calculated the concentration profiles (which are like those shown in Fig. 7) for various T_{max} and v_T values, and C_e values were determined for each set of T_{max} and v_T. These are plotted in Fig. 8 together with the experimental results. Parts (a), (c) and (e) of Fig. 8 show the relationship between the C_e of chemicals and T_{max} for v_T values of 0.0167, 0.05 and 0.10 K/s, respectively. Parts (b), (d) and (f) of Fig. 8 show magnified vertical axes of Fig. 8(a), (c) and (e), respectively. They elucidate the concentration profiles of cellulose and oligomers. As shown in Fig. 8, at a low T_{max}, a reasonable agreement is obtained between the calculated results and the experimental data. However, when T_{max} is greater than 533 K, the calculated lines for the pyrolysis products stray away from the experimentally obtained data. This tendency is more marked under lower v_T conditions. It is thought that this gap between the experimental data and the calculated result is caused by the formation of tar, which is disregarded in the proposed model. The effect of tar formation on the modeling of cellulose decomposition, which was not investigated in this study which focused on the liquefaction of cellulose, is a subject for further work. Although the calculated results for pyrolysis products stray from the experimental data for T_{max} values over ~533 K, the calculated results are reliable in the range where T_{max} is lower than 533 K. In addition, the calculated results for cellulose, oligomer and monomer are reliable over the whole range of T_{max} values investigated, because they probably do not participate in the formation of tar. The correlation coefficients for all results at $T_{max} < 533$ K investigated in this study are listed in Table 3.

We next investigated the effect of the heating rate on the modeling of cellulose liquefaction in hot compressed water by using the proposed mathematical model. As shown in Fig. 8, as the heating rate becomes slow, both the calculated line and the experimental data shift to the left. This indicates that the

Table 3
Correlation coefficients between experimental data and calculated results on the relationship between $C_{e,i}$ and T_{max}

v_T (K/s)	Cellulose	Oligomer	Monomer	Pyrolysis
0.0167	0.987	0.382	0.905	0.872
0.033	0.956	0.581	0.992	0.877
0.05	0.985	0.660	0.997	0.932
0.067	0.906	0.933	0.993	0.861
0.10	0.941	0.876	0.993	0.970
0.167	0.914	0.966	0.995	0.987

proposed model reflects the temperature dependence during the reaction well. Fig. 9 shows the calculated results for cellulose decomposition at various heating rates when $T_{max} = 523$ K. From this figure, it is evident that the concentration profile of cellulose is strongly affected by the heating rate when the heating rate is below 1 K/s. A heating rate of 1 K/s is difficult to actualize even in the process using in this study; a completely small batch reactor with an electric heater. Although a large volume reactor is necessary to treat wood biomass in large quantities, it is more difficult to achieve rapid heating of contents with a large volume. That is to say, in the practical operation, the heating and quenching processes significantly affect the liquefaction of wood biomass. For such a large plant, by using the mathematical model proposed in this study, we can also predict the desirable operation conditions and the concentration of chemicals of the output.

Meanwhile, the mathematical model proposed in this study is also useful for a process with a flow-type reactor. If the temperature distribution of fluid along the current in a tubular-flow reactor is known, one can estimate the concentrations of the reactants at any position in the reactor by using the proposed mathematical model. According to the estimated concentration profile, the concentration of products can be controlled by adjusting the reactor length.

In either case, the mathematical model proposed in this study provides basic information for the design of hot compressed water liquefaction reactors.

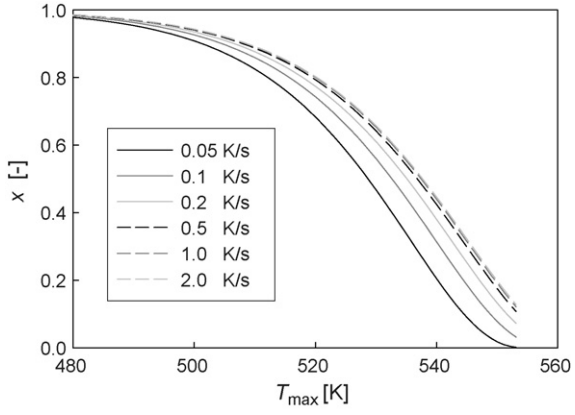

Fig. 9. Relationship between decomposition ratio of cellulose and T_{max} for various heating rates.

4. Conclusion

In this study, we investigated cellulose liquefaction in hot compressed water by using a batch type reactor, which is preferred for the treatment of solid wood biomass, but requires slow heating and quenching processes. It was found that cellulose liquefaction was affected by the heating rate. Under identical maximum temperature conditions, the amount of cellulose decomposed increased as the heating rate decreased. This same tendency was observed for the reaction of monosaccharides and pyrolysis products. From the experimental data, the mechanism of cellulose liquefaction was estimated to be as follows: stepwise decomposition from 1, cellulose to oligosaccharides; 2, oligosaccharides to monosaccharides and pyrolysis products; and 3, monosaccharides to pyrolysis products. A mathematical model which calculated cellulose decomposition, taking into account the temperature variation over time, was derived according to the estimated reaction mechanism. The proposed model provided reasonable concentration profiles for maximum temperatures below about 533 K. It also described the effect of the heating rate on the overall result for the cellulose decomposition reaction well. The calculated results for various heating rates show that it is necessary to consider the effect of the heating rate when the heating rate of the system is below 1 K/s. The mathematical model proposed in this study provides basic information for the design of batch type reactors as well as flow type reactors for hot compressed water liquefaction.

Acknowledgment

This study was supported in part by a Grant-Aid from The Ministry of Education, Culture, Sports, Science and Technology of Japan.

References

[1] M. Modell, R.C. Reid, S. Amin, Gasification Process, US Patent 4,113,446 (September 12, 1978).
[2] L.J. Sealock Jr., D.C. Elliott, E.G. Baker, R.S. Butner, Chemical processing in high-pressure aqueous environments. 1. Historical perspective and continuing developments, Ind. Eng. Chem. Res. 32 (1993) 1535–1541.
[3] I.-G. Lee, M.-S. Kim, S.-K. Ihm, Gasification of glucose in supercritical water, Ind. Eng. Chem. Res. 41 (2002) 1182–1188.
[4] D. Yu, M. Aihara, M.J. Antal Jr., Hydrogen production by steam reforming glucose in supercritical water, Energy Fuels 7 (1993) 574–577.
[5] X. Xu, Y. Matsumura, J. Stenberg, M.J. Antal Jr., Carbon-catalyzed gasification of organic feedstocks in supercritical water, Ind. Eng. Chem. Res. 35 (1996) 2522–2530.
[6] M.J. Antal Jr., G. Várhegyi, E. Jakab, Cellulose pyrolysis kinetics: revisited, Ind. Eng. Chem. Res. 37 (1998) 1267–1275.
[7] M.J. Antal Jr., S.G. Allen, D. Schulman, X. Xu, Biomass gasification in supercritical water, Ind. Eng. Chem. Res. 39 (2000) 4040–4053.
[8] T. Adschiri, S. Hirose, R. Malaluan, K. Arai, Noncatalytic conversion of cellulose in supercritical and subcritical water, J. Chem. Eng. Jpn. 26 (1993) 676–680.
[9] T. Sakaki, M. Shibata, T. Miki, H. Hirosue, N. Hayashi, Decomposition of cellulose in near-critical water and fermentability of the products, Energy Fuels 10 (1996) 684–688.
[10] T. Minowa, F. Zhen, T. Ogi, G. Várhegyi, Decomposition of cellulose and glucose in hot-compressed water under catalyst-free conditions, J. Chem. Eng. Jpn. 31 (1998) 131–134.

[11] H. Ando, T. Sasaki, T. Kokusho, M. Shibata, Y. Uemura, Y. Hatate, Decomposition behavior of plant biomass in hot-compressed water, Ind. Eng. Chem. Res. 39 (2000) 3688–3693.
[12] W.S.L. Mok, M.J. Antal Jr., Uncataluzed solvolysis of whole biomass hemicellulose by hot compressed liquid water, Ind. Eng. Chem. Res. 31 (1992) 1157–1161.
[13] O. Bobleter, R. Vidotti, A. Zemann, W. Prutsch, Hydrothermal pretreatment of bagasse and wheat straw. biomass for energy and industry, in: G. Grassi, G. Gosse, G. dos Santos (Eds.), Proceedings of the Fifth E.C. Conference Volume 2 Conversion and Utilisation of Biomass, Elsevier Applied Science: London, 1990, pp. 2.31–2.37.
[14] A. Zemann, O. Bobleter, W. Prutsch, Hydrothermolysis—a pretreatment process for pulp production. In lignocellulosics: science, technology, development and use, in: J.F. Kennedy, G.O. Philips, P.A. Williams (Eds.), Ellis Horwood Series in Polymer Science and Technology, Ellis Horwood, Chichester, UK, 1992, pp. 213–226.
[15] S.G. Allen, L.C. Kam, A.J. Zemann, M.J. Antal Jr., Fractionation of sugar cane with hot, compressed, liquid water, Ind. Eng. Chem. Res. 35 (1996) 2709–2715.
[16] M. Sasaki, B. Kabyemela, R. Malaluan, S. Hirose, N. Takeda, T. Adschiri, K. Arai, Cellulose hydrolysis in subcritical and supercritical water, J. Supercrit. Fluids 13 (1998) 261–268.
[17] M. Sasaki, Z. Fang, Y. Fukushima, T. Adschiri, K. Arai, Dissolution and hydrolysis of cellulose in subcritical and supercritical water, Ind. Eng. Chem. Res. 39 (2000) 2883–2890.
[18] M. Sasaki, T. Adschiri, K. Arai, Kinetics of cellulose conversion at 25 MPa in sub- and supercritical water, AIChE J. 50 (2004) 192–202.
[19] M. Sasaki, M. Furukawa, K. Minami, T. Adschiri, K. Arai, Kinetics and Mechanism of Cellobiose Hydrolysis and Retro-Aldol Condensation in Subcritical and Supercritical Water, Ind. Eng. Chem. Res. 41 (2002) 6642–6649.
[20] M. Sasaki, PhD thesis, Tohoku University, Sendai, Japan, 2000.
[21] B.M. Kabyemela, T. Adschiri, R.M. Malaluan, K. Arai, Kinetics of glucose epimerization and decomposition in subcritical and supercritical water, Ind. Eng. Chem. Res. 36 (1997) 1552–1558.
[22] B.M. Kabyemela, T. Adschiri, R.M. Malaluan, K. Arai, Degradation kinetics of dihydroxyacetone and glyceraldehyde in subcritical and supercritical water, Ind. Eng. Chem. Res. 36 (1997) 2025–2030.
[23] S. Amin, R.C. Reid, M. Modell, Reforming and decomposition of glucose in an aqueous phase. Intersociety Conference on Environmental Systems, San Francisco, CA, 1975, The American Society of Mechanical Engineers (ASME), New York, 1975, ASME paper No. 75-ENAs-21.
[24] O. Bobleter, G. Pape, Hydrothermal decomposition of glucose, Monatsh. Chem. 99 (1968) 1560–1567.
[25] Y. Matsumura, S. Yanachi, T. Yoshida, Glucose decomposition kinetics in water at 25 MPa in the temperature range of 448–673 K, Ind. Eng. Chem. Res. 45 (2006) 1875–1879.
[26] G.E. Walrafen, W.-H. Yang, Y.C. Chu, Raman spectra from saturated water vapor to the supercritical fluid, J. Phys. Chem. B 103 (1999) 1332–1338.
[27] N. Ohtomo, K. Tokiwano, K. Arakawa, The structure of liquid water by neutron scattering. II. Temperature dependence of the liquid structure, Bull. Chem. Soc. Jpn. 55 (1982) 2788–2895.
[28] K. Yoshida, C. Wakai, N. Matubayasi, M. Nakahara, A new high-temperature multinuclear-magnetic-resonance probe and the self-diffusion of light and heavy water in sub- and supercritical conditions, J. Chem. Phys. 123 (2005) 164506/1–164506/10.